Centrum voor Wiskunde en Informatica
REPORT*RAPPORT*

Diffusive Gradients in the PTS System

J.G. Blom, M.A. Peletier

Modelling, Analysis and Simulation (MAS)

MAS-R0020 July 31, 2000

Report MAS-R0020
ISSN 1386-3703

CWI
P.O. Box 94079
1090 GB Amsterdam
The Netherlands

Diffusive Gradients in the PTS System

J. G. Blom and Mark A. Peletier
CWI
P.O. Box 94079, 1090 GB Amsterdam, The Netherlands

ABSTRACT
It has recently been conjectured that metabolic pathways with membrane-bound enzymes can give rise to concentration gradients in the cytosolic pathway components. We investigate this issue using a theoretical model for the Phosphoenolpyruvate-dependent Phosphotransferase system in *E. coli*, for which accurate measurements of the kinetic parameters are available. We show that significant spatial gradients indeed exist, and we discuss the potential implications of this finding.

2000 Mathematics Subject Classification: Primary: 92C40. Secondary: 35J55, 65C20, 92-04.
1998 ACM Computing Classification System: J.3 and G.1.8.
Keywords and Phrases: Protein kinase, phosphatase, spatial localisation, diffusion, cellular gradients.
Note: Work carried out under project MAS1.3 - Applications from the Life Sciences.

1. Introduction

Bacteria such as *E. coli* have relatively little interior structure. The cell contains no interior divisions, and the cytoplasm is free to move throughout the cell. In combination with the relatively small size of *E. coli* this has led to an assumption, which is common in the biochemical literature, that the inside of the cell behaves as a 'well-stirred reactor': i.e., the concentrations of those chemical species that are not membrane-bound can be assumed to be constant throughout the cell, and to remain so during any reactions that they may undergo.

While there are many situations in which such an assumption may be justified, we will concentrate here on an exception to this rule. The Phosphoenolpyruvate-dependent Phosphotransferase system (PTS), described in detail below, is a pathway that is partly cytoplasmic, partly membrane-bound. The pathway is dependent on diffusion for the transport between the cytoplasm and the membrane; this implies that a spatial gradient in the concentration of some of the species is needed to achieve the necessary pathway flux. Our goal in this paper is to model the PTS system in a comprehensive manner, taking into account the detailed reaction mechanism of [5, 6], the spatial separation that is created by binding one of the proteins to the cell membrane, and the diffusion process that is responsible for the transport to and from the membrane. We will show that the resulting concentration gradients are significant (in line with the suggestions of [2]) and we shall make some suggestions for an experimental verification of this fact.

In the next two sections we will describe the PTS system and the assumptions we make for the model we have investigated. In Sections 4 and 5 we briefly describe the numerical methods that we have used to calculate solutions for this model, and the results that we obtain for various model experiments. Finally we discuss whether these results are experimentally verifiable.

2. The PTS System

The Phosphoenolpyruvate-dependent Phosphotransferase system (PTS) is an essential element in the glucose metabolism of *E. coli*. Its two main functions are to transport extracellular glucose (Glc) through the membrane and to simultaneously attach to it a phosphoryl group (PO_3).

The phosphoryl group is originally derived from phosphoenolpyruvate (PEP), and is passed to the glucose molecule via a pathway of protein–protein interactions. A simplified reaction mechanism is

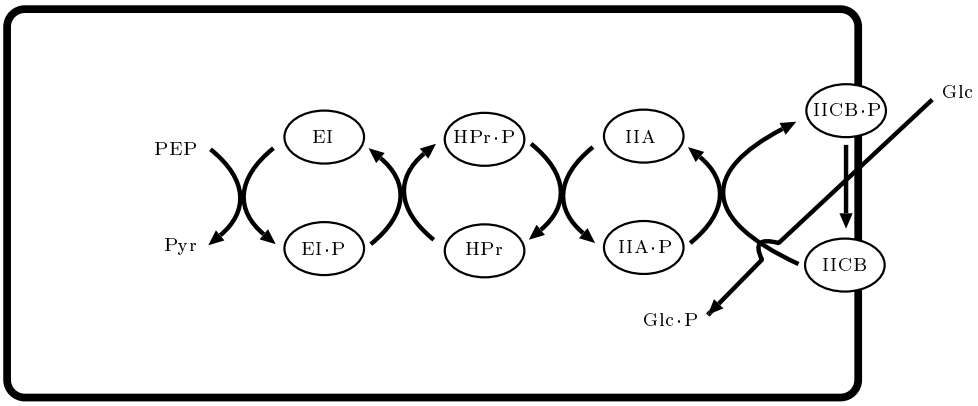

Figure 1: A schematic representation of the PTS system. The ellipses represent proteins, the other metabolites are smaller molecules.

shown in Figure 1. Each pair of arrows represents a pair of chemical reactions; for instance, the leftmost reaction, in which PEP passes a phosphoryl group to Enzyme I (EI), creating EI·P and pyruvate (Pyr), might be written more explicitly

$$\mathrm{EI} + \mathrm{PEP} \underset{k_{-1}}{\overset{k_1}{\rightleftarrows}} \mathrm{EI{\cdot}P{\cdot}Pyr} \underset{k_{-2}}{\overset{k_2}{\rightleftarrows}} \mathrm{EI{\cdot}P} + \mathrm{Pyr} \tag{2.1}$$

Throughout this paper we assume that reaction rates follow the law of mass action, so that (2.1) also defines the reaction rates as $k_1[\mathrm{EI}][\mathrm{PEP}] - k_{-1}[\mathrm{EI{\cdot}P{\cdot}Pyr}]$ and $k_2[\mathrm{EI{\cdot}P{\cdot}Pyr}] - k_{-2}[\mathrm{EI{\cdot}P}][\mathrm{Pyr}]$. Similarly, the other reactions, involving HPr, domain A of Enzyme II (IIA), and domains B-C of Enzyme II (IICB), have the explicit form

$$\mathrm{EI{\cdot}P} + \mathrm{HPr} \underset{k_{-3}}{\overset{k_3}{\rightleftarrows}} \mathrm{EI{\cdot}P{\cdot}HPr} \underset{k_{-4}}{\overset{k_4}{\rightleftarrows}} \mathrm{EI} + \mathrm{HPr{\cdot}P} \tag{2.2}$$

$$\mathrm{HPr{\cdot}P} + \mathrm{IIA} \underset{k_{-5}}{\overset{k_5}{\rightleftarrows}} \mathrm{HPr{\cdot}P{\cdot}IIA} \underset{k_{-6}}{\overset{k_6}{\rightleftarrows}} \mathrm{HPr} + \mathrm{IIA{\cdot}P} \tag{2.3}$$

$$\mathrm{IIA{\cdot}P} + \mathrm{IICB} \underset{k_{-7}}{\overset{k_7}{\rightleftarrows}} \mathrm{IIA{\cdot}P{\cdot}IICB} \underset{k_{-8}}{\overset{k_8}{\rightleftarrows}} \mathrm{IIA} + \mathrm{IICB{\cdot}P} \tag{2.4}$$

$$\mathrm{IICB{\cdot}P} + \mathrm{Glc} \underset{k_{-9}}{\overset{k_9}{\rightleftarrows}} \mathrm{IICB{\cdot}P{\cdot}\,Glc} \underset{k_{-10}}{\overset{k_{10}}{\rightleftarrows}} \mathrm{IICB} + \mathrm{Glc{\cdot}P} \tag{2.5}$$

The geometry of the pathway in the cell is schematically indicated in Figure 1:

1. The proteins IICB (and its alternative forms, IICB·P, IIA·P·IICB, and IICB·P·Glc) are fixed to the cell membrane;
2. All species to the left of IICB/IICB·P in (1) (i.e., PEP, Pyr, EI, HPr, IIA, and their various combinations and alternative forms) are confined to the interior of the cell;
3. Glucose is transported from outside to inside, so Glc is supposed only to be present outside of the cell, while Glc·P is confined to the inside.

This spatial separation between EI, HPr, and IIA on one hand and IICB on the other hand implies that an element of spatial transport is necessary to bring reacting species into contact with each other. In this paper we shall assume that this transport is effectuated by (passive) diffusion.

REMARK 2.1 In what follows we implicitly adopt the continuum hypothesis, i.e., we assume that the behaviour of the set of molecules in the cell can be modelled by considering a continuous representation (a concentration). That this is possible is not completely trivial, and depends simply stated on the number of molecules that are present in the cell. For a spherical cell of radius 1 μm, each μM of concentration is equivalent to 2500 molecules inside a single cell. With the concentrations that we use here (Table 4) the cytosolic species are counted in tens of thousands. The membrane concentration of IICB of 3.33 μM μm corresponds to 25000 molecules. We conclude that the continuum hypothesis is a reasonable assumption.

Thus we model the time variation of each of the interior unknown species by equations of the form

$$\frac{\partial A}{\partial t} - \nabla(D_A.\nabla A) = R_A \qquad \text{for } (x,t) \in \Omega \times (0,\infty), \tag{2.6}$$

where A is the volume concentration of any one of the species EI, EI·P·Pyr, EI·P, EI·P·HPr, HPr, HPr·P, HPr·P·IIA, IIA, and IIA·P. The coefficients D_A are the corresponding diffusion rates, to which we shall return later, and the reaction rates are given by

$$\begin{array}{llllll} R_{\mathrm{EI}} & = J_4 - J_1 & R_{\mathrm{EI\cdot P\cdot HPr}} & = J_3 - J_4 & R_{\mathrm{HPr\cdot P\cdot IIA}} & = J_5 - J_6 \\ R_{\mathrm{EI\cdot P\cdot Pyr}} & = J_1 - J_2 & R_{\mathrm{HPr}} & = J_6 - J_3 & R_{\mathrm{IIA}} & = -J_5 \\ R_{\mathrm{EI\cdot P}} & = J_2 - J_3 & R_{\mathrm{HPr\cdot P}} & = J_4 - J_5 & R_{\mathrm{IIA\cdot P}} & = J_6 \end{array} \tag{2.7}$$

Each of the J_i refers to the total reaction rate in equation i, including both forward and backward reactions. For reference we list them explicitly:

$$\begin{array}{ll} J_1 = k_1[\mathrm{EI}][\mathrm{PEP}] - k_{-1}[\mathrm{EI\cdot P\cdot Pyr}] & J_4 = k_4[\mathrm{EI\cdot P\cdot HPr}] - k_{-4}[\mathrm{EI}][\mathrm{HPr\cdot P}] \\ J_2 = k_2[\mathrm{EI\cdot P\cdot Pyr}] - k_{-2}[\mathrm{EI\cdot P}][\mathrm{Pyr}] & J_5 = k_5[\mathrm{HPr\cdot P}][\mathrm{IIA}] - k_{-5}[\mathrm{HPr\cdot P\cdot IIA}] \\ J_3 = k_3[\mathrm{EI\cdot P}][\mathrm{HPr}] - k_{-3}[\mathrm{EI\cdot P\cdot HPr}] & J_6 = k_6[\mathrm{HPr\cdot P\cdot IIA}] - k_{-6}[\mathrm{HPr}][\mathrm{IIA\cdot P}] \end{array} \tag{2.8}$$

The species IICB, IIA·P·IICB, IICB·P, and IICB·P· Glc, which are confined to the cell membrane, are modelled by surface concentrations defined on the boundary of the domain, $\partial\Omega$. They are also assumed to undergo diffusion, as well as reaction:

$$\frac{\partial B}{\partial t} - \nabla(D_B.\nabla B) = R_B, \qquad \text{for } (x,t) \in \partial\Omega \times (0,\infty), \tag{2.9}$$

where the reaction rate R_B is given by

$$\begin{array}{llll} R_{\mathrm{IICB}} & = J_{10} - J_7 & R_{\mathrm{IICB\cdot P}} & = J_8 - J_9 \\ R_{\mathrm{IIA\cdot P\cdot IICB}} & = J_7 - J_8 & R_{\mathrm{IICB\cdot P\cdot\ Glc}} & = J_9 - J_{10} \end{array} \tag{2.10}$$

Here the relevant reaction rates are given by

$$\begin{array}{ll} J_7 = k_7[\mathrm{IIA\cdot P}][\mathrm{IICB}] - k_{-7}[\mathrm{IIA\cdot P\cdot IICB}] & J_9 = k_9[\mathrm{IICB\cdot P}][\mathrm{Glc}] - k_{-9}[\mathrm{IICB\cdot P\cdot\ Glc}] \\ J_8 = k_8[\mathrm{IIA\cdot P\cdot IICB}] - k_{-8}[\mathrm{IIA}][\mathrm{IICB\cdot P}] & J_{10} = k_{10}[\mathrm{IICB\cdot P\cdot\ Glc}] - k_{-10}[\mathrm{IICB}][\mathrm{Glc\cdot P}] \end{array} \tag{2.11}$$

Note that since the concentrations [IICB], [IIA·P·IICB], [IICB·P], and [IICB·P· Glc] are surface concentrations (L^{-2}) rather than volume concentrations (L^{-3}), the rates J_7–J_{10} are also per unit surface. In these expressions [IIA], [IIA·P], [Glc], and [Glc·P] are interpreted as the values of the volume concentrations at the location of the boundary.

For the mass balance of the interior species the reaction at the boundary represents a source/sink term. The corresponding boundary condition is obtained by equating the source/sink with the local

flux at the boundary:

$$\begin{aligned} &D_A \frac{\partial}{\partial \nu} A = 0, \qquad A = \text{EI},\ \text{EI}\cdot\text{P}\cdot\text{Pyr},\ \text{EI}\cdot\text{P},\ \text{EI}\cdot\text{P}\cdot\text{HPr},\ \text{HPr}, \text{HPr}\cdot\text{P},\ \text{HPr}\cdot\text{P}\cdot\text{IIA}, \\ &D_{\text{IIA}} \frac{\partial}{\partial \nu}[\text{IIA}] = J_8, \qquad D_{\text{IIA}\cdot\text{P}} \frac{\partial}{\partial \nu}[\text{IIA}\cdot\text{P}] = -J_7 \end{aligned} \tag{2.12}$$

Note that the difference in dimensions between J_7-J_{10} and the other rates implies that such a boundary condition is dimensionally correct. If the local (thermal) diffusion of the species is unchanged by the fixture to the membrane, then the same rate coefficients k_i and k_{-i} apply as in a voluminal context.

The concentrations of PEP, Pyr, Glc, and Glc $\cdot$ P are held constant, and we will treat these as parameters in the sequel. If we supplement (2.6)-(2.12) with initial conditions for all species, then the system has a unique solution that remains bounded for all time $t > 0$. In this paper, however, we are interested in stationary states. We conjecture that the system (2.6)-(2.12) has a unique stationary state, which is globally attracting; all our numerical results support this conjecture.

3. Questions of symmetry

The cell will be taken to be three-dimensional and spherical. All concentrations of cytoplasmic species are considered to be functions of the spatial variable, and the membrane-bound species are defined on the boundary of the sphere.

In the more general of our simulations, no symmetry was pre-imposed on the solutions. However, provided all parameters respected the radial symmetry, we found no evidence of symmetry-breaking: all solutions were radially symmetric (note, however, that if a parameter such as Glc is non-symmetric, then solutions of the equations will also be non-symmetric). In the following sections we will therefore describe the problem and the results completely in terms of the radial variable.

One might speculate on modifications of the model that *would* allow for symmetry breaking. The first was mentioned above: if any of the data of the problem is non-symmetric, then the solution will not be radially symmetric either. A different example of a similar phenomenon would be if one of the species (e.g. IIA) would play a role in a different reaction mechanism, and if this other mechanism itself would be non-symmetrically distributed throughout the cell.

In yeast a phenomenon is observed in which membrane-bound proteins spread over the membrane while they are active, (i.e., while the flux is non-zero), but coagulate when they become inactive, even leading to large clumps that are degraded by the cell. A phenomenon of this type might lead to interesting (time-dependent) behaviour.

4. Numerical Methods

In spherical symmetry equations (2.6) reduce to the following one-dimensional system of reaction-diffusion equations in the interior of the cell:

$$\frac{\partial c}{\partial t} = R_c + \frac{1}{r^2}\frac{\partial}{\partial r}(r^2 D_c(r)\frac{\partial c}{\partial r}), \qquad \text{for } (r,t) \in (0,\text{R}) \times (0,\infty), \tag{4.1}$$

for the species $c = \text{EI},\ \text{EI}\cdot\text{P}\cdot\text{Pyr},\ \text{EI}\cdot\text{P}, \text{EI}\cdot\text{P}\cdot\text{HPr},\ \text{HPr}, \text{HPr}\cdot\text{P},\ \text{HPr}\cdot\text{P}\cdot\text{IIA},\ \text{IIA},\ \text{IIA}\cdot\text{P}$, where R_c is given by (2.7) and (2.8). The boundary conditions are a symmetry condition in the center,

$$\frac{\partial c}{\partial r} = 0, \qquad \text{for } r = 0, \tag{4.2}$$

and equation (2.12) at the membrane.

In the cell membrane the system of diffusion-reaction PDEs (2.9) translates for the radially symmetric case to a system of ODEs

$$\frac{\partial b}{\partial t} = R_b, \qquad \text{for } t \in (0,\infty), \tag{4.3}$$

where b = IICB, IIA·P·IICB, IICB·P, IICB·P· Glc (which is now a scalar function of time only), and R_b is given by (2.10) and (2.11).

We solve system (4.1)-(4.3) using the Method of Lines: the spatial derivatives are discretized on a computational grid, and the resulting system of ODEs is integrated in time. The variables of the ODEs are the protein concentrations. Positivity and mass conservation are characteristic properties of the continuous variables and should thus be mimicked by the computational solution.

The discretization in space is straightforward: The spatial interval is divided into N equal subintervals of length $\Delta r = \frac{\mathrm{R}}{N}$, and in each subinterval the solutions are taken constant. We approximate the diffusion term in (4.1) by

$$\frac{1}{r_i^2}\frac{r_{i+1/2}^2 F_c(r_{i+1/2}) - r_{i-1/2}^2 F_c(r_{i-1/2})}{\Delta r}. \tag{4.4}$$

For computational cell boundaries $r_{i+1/2}$ in the interior of the cell the diffusive flux over the boundary is given by

$$F_c(r_{i+1/2}) = D_c(r_{i+1/2})\frac{c_{i+1} - c_i}{\Delta r}, \qquad \text{for } i = 1, ..., N-1, \tag{4.5}$$

and at the boundaries of the computational domain the flux is given by (cf. (4.2))

$$F_c(r_{1/2}) = 0$$

and (cf. (2.12))

$$\begin{aligned} &F_c(r_{N+1/2}) = 0, \qquad \text{for all species except IIA and IIA·P,} \\ &F_{\mathrm{IIA}}(r_{N+1/2}) = J_8 = k_8[\mathrm{IIA{\cdot}P{\cdot}IICB}] - k_{-8}[\mathrm{IIA}]_N[\mathrm{IICB}], \qquad \text{and} \\ &F_{\mathrm{IIA{\cdot}P}}(r_{N+1/2}) = -J_7 = -(k_7[\mathrm{IIA{\cdot}P}]_N[\mathrm{IICB}] - k_{-7}[\mathrm{IIA{\cdot}P{\cdot}IICB}]). \end{aligned}$$

For the choice of a time integrator it is important to realize that the system of ODEs obtained after semi-discretization is moderately stiff. Eigenvalues of the reaction system range between -10^7 and 0 for the wild-type *in vivo* concentration values and the kinetic rate constants given in [6]. If one would integrate such a stiff system in time with an explicit scheme this would lead to time steps in the order of 10^{-7}, even when the solution is close to steady-state. Therefore it is necessary to use an implicit time-integrator, in our case the off-the-shelf solver DASSL[1, 3]. DASSL is a variable-step variable-order BDF method. When the order is restricted to one it results in the familiar Backward-Euler method, which is the only known implicit method which combines positivity and mass conservation. In our experiments we also allowed higher order BDF schemes; negative concentrations did not occur.

5. Experiments

In [5, 6] PTS model experiments are described in a 'stirred-tank' setting, i.e. diffusion is neglected, there is no spatial separation, and all reactants are assumed to be spread homogeneously in space. In this paper we are interested in the more general setup described above, with an emphasis on the influence of diffusive transport on the steady-state pathway flux. In this section we describe a number of numerical experiments in which we vary the diffusion coefficients. We not only consider the spatial gradients in the species concentration and the distribution over the various protein forms (unphosphorylated, phosphorylated, complex), but also the influence on the uptake of glucose, viz. the flux through the membrane given by (2.11), and the flux-response coefficients. The latter describe the dependence of the flux on the various protein concentrations and diffusion coefficients and are defined by

$$R_p^J = \frac{\partial \ln |J|}{\partial \ln p}, \tag{5.1}$$

where J is the membrane flux in steady-state and p the dependence parameter.

For the geometry of the cell we assume a sphere with a radius of 1 μm. The total protein concentrations and the kinetic parameters are those of [6, for the concentrations the *in vivo* values]. For the membrane-bound protein IICB a translation has to be made, since in [6] this protein was represented by a bulk concentration (10 μM). We calculate the boundary (surface) concentration by multiplying the bulk concentration by the volume-surface ratio $(4/3)\pi r^3/4\pi r^2$. As mentioned above, the kinetic constants related to boundary metabolites, which where determined for bulk concentrations in [6], apply unchanged when one of the metabolites in the reaction is fixed to the membrane. For the sake of completeness the parameter values are listed in Table 4 in the Appendix. In all our experiments we used a uniform grid of 1000 cells. Fifty cells would in fact be sufficient for a good indication of the spatial distribution of the concentrations; however, the values of the flux and the flux-response coefficients are very sensitive to the gradient of the solution near the boundary, and an accurate computation of these quantities therefore requires a dense spatial discretization near the boundary.

As is to be expected, in the limit $D_c \to \infty$ the protein concentrations show no spatial gradients, and the simulated concentration values as well as the flux and flux-response coefficients equal those of [6].

In the first model experiment, marked **A** in the sequel, the diffusion parameter D_c is constant in space and equal for all protein species to 60 μm^2 min^{-1} (cf. [4]). As can be seen in Figure 2 the protein concentrations show gradients, but the total protein concentration for each of the three cytosolic types EI, HPr, and IIA (e.g., in the first diagram the combination EI + EI·P + EI·P·Pyr + EI·P·HPr), is constant in space. This can be explained by the fact that the PDE for the sum, which is obtained by adding the 4 PDEs for the various subspecies, has the form

$$\frac{\partial c}{\partial t} - \nabla (D_c . \nabla c) = 0,$$

since $D_c = D$ is independent of the subspecies, and since the reaction terms R_c cancel each other (conservation of the protein). With the accompanying boundary conditions the only steady states for this equation are constants.

In experiment **B** the effect is shown of a space dependency of D_c. The cell is divided (conceptually) into two parts, an inner region ($0 \le r \le 0.5\,\mu$m) and an outer region ($0.5\,\mu\text{m} \le r \le 1\,\mu$m). The diffusion coefficient in the outer region is equal to the value above, and in the inner region we adopted a value that is lower by a factor of 50. This assumption is inspired by the higher concentration of DNA in the inner region, which creates an environment in which globular particles diffuse more slowly. The results can be found in Figure 3.

The effects of varying the diffusion coefficients among the different subspecies is clearly seen in Figure 4, where we assume that complexes diffuse at a lower rate than uncomplexed proteins. The diffusion coefficient for uncomplexed proteins is the same as in experiment **A** while the coefficient for complexes is taken a factor 1000 lower. Now the summed concentrations of the various subspecies (e.g., EI + EI·P + EI·P·Pyr + EI·P·HPr) also show clear spatial gradients.

The factor of 1000 has the merit of clearly demonstrating the effect of variation among subspecies, but it does not provide a meaningful comparison to the actual system. For an estimate of realistic values of the various diffusion coefficients we make the following assumptions:

- proteins (and complexes) are spheres,
- D varies linearly with the inverse of the radius of that sphere (as in the Stokes-Einstein relationship),
- the volume of the sphere varies linearly with the mass of the protein species, and
- the mass of the phosphoryl group and of pyruvate is negligible (M(EI) = 63.5kDa, M(HPr) = 9.1kDa, M(IIA) = 18.2kDa).

This leads to the following values of D_c:

$$\begin{array}{llllll} D_{\mathrm{EI}} & = 1/1.91 \cdot D_{\mathrm{HPr}} & D_{\mathrm{HPr}} & = 60\,\mu\mathrm{m}^2\ \mathrm{min}^{-1} & D_{\mathrm{IIA}} & = 1/1.26 \cdot D_{\mathrm{HPr}} \\ D_{\mathrm{EI\cdot P\cdot Pyr}} & = D_{\mathrm{EI}} & D_{\mathrm{EI\cdot P\cdot HPr}} & = 1/2.00 \cdot D_{\mathrm{HPr}} & D_{\mathrm{HPr\cdot P\cdot IIA}} & = 1/1.44 \cdot D_{\mathrm{HPr}} \\ D_{\mathrm{EI\cdot P}} & = D_{\mathrm{EI}} & D_{\mathrm{HPr\cdot P}} & = D_{\mathrm{HPr}} & D_{\mathrm{IIA\cdot P}} & = D_{\mathrm{IIA}} \end{array} \quad (5.2)$$

The result of this choice for the diffusion coefficients is shown in Figure 5.

One can also mimic the situation where a large label is attached to one of the smaller proteins such as HPr or IIA. In our experiments we enlarged the mass of the specific protein by a factor of 10 and changed the diffusion coefficients accordingly. The result can be seen in Figures 6 and 7 for the proteins HPr and IIA.

For all these model experiments we give the distribution of the membrane protein species in Table 1 and the steady-state properties (the flux and the flux-response coefficients) of the model in Table 2. For comparison with the 'stirred-tank' *in vivo* experiment of [6] we list for $D_c = 10^5\,\mu\mathrm{m}^2\ \mathrm{min}^{-1}$ the intracellular species distribution in Table 3, the membrane species values in Table 1 and the flux and flux-response coefficients in Table 2.

Although the distribution over the protein species, when averaged over space, is roughly the same as in the experiments of Rohwer et al., we see from Table 2 that the flux in a situation without gradients, the stirred-tank approximation or 'infinite' diffusion, is significantly higher than in any of the other experiments, all giving rise to more or less large gradients of the protein species. And where the stirred-tank approximation leads to the conclusion that the flux is merely dependent on $[\mathrm{IICB}]_{total}$ a model with diffusion makes the uptake of glucose also dependent on $[\mathrm{EI}]_{total}$ and even more on $[\mathrm{IIA}]_{total}$. The actual values of the various diffusion coefficients seem to be of less importance. Only in a few cases this is also of influence on the uptake values (flux and flux-response coefficients). E.g., if we look at the flux values in Table 2 a spatial dependence of D (exp. **B**) is of no influence, but the assumption that complexes are 'immobile' compared to uncomplexed proteins (exp. **C**) leads to a much larger flux. This choice gives rise to the largest gradients, also in the total concentrations, and to the largest flux. Interesting from an experimental point of view are **E** and **F**. In **E** we have the situation that attaching a large label to HPr gives rise to a noticeable gradient in $[\mathrm{IIA}]_{total}$ without changing the up-take values too much. In **F**, where a large label is attached to IIA, we predict a much smaller flux.

6. Discussion

In this paper we discuss the effects of extending the kinetic PTS model of [5, 6] with spatial transport modelled by diffusion. Experiments with this model show that, in line with the assertions of [2], diffusion gives rise to large gradients in the concentrations of the various protein species and to a different prediction for the uptake of glucose compared with the results in [6].

In [2] the authors state that 'Large cellular gradients of the phosphorylated and unphosphorylated form of proteins would have very important implications for cell signalling'. While we intend to leave this point to a later and more comprehensive discussion, a first remark can already be made on the basis of Table 2. In the well-stirred case the flux control is overwhelmingly localized in the concentration of IICB; the addition of diffusion transfers part of this control to EI and IIA, thus more than doubling the flux-response coefficient for both proteins.

Turning towards a comparison with experimental data, a first interesting question arises in conjunction with the *in vivo* experimental data of [6]. The observed values of the pathway flux were higher than those calculated in the model experiments in [6], which in turn are higher than those that are predicted by the current model. The fact that addition of diffusion to the model takes us further from experimental data is intriguing, and this issue remains to be resolved.

An independent question is whether it is possible to find experimental proof that such concentration gradients as discussed above exist *in vivo*. The simplest experiment to measure gradients would consist of labeling a protein such as IIA; with such an experiment one would measure the sum of the

four subspecies, i.e., IIA + IIA·P + HPr·P·IIA + IIA·P·IICB. The thick line in Figure 5 shows the concentration of this combination. While there is a slight variation in space, it does not seem strong enough to be detected among a significant amount of noise.

By labeling two proteins by different fluorescent labels, and detecting energy transfer from one to the other, one can (theoretically) detect complexes of these two proteins. If this technique could be applied to, for instance, HPr·P·IIA, then the resulting response would be strong enough to persist through perturbations (see Figure 5). This is an avenue that is currently being explored.

A third possibility would be not to measure the gradients directly but at least prove their existence in an indirect manner. The existence of a concentration gradient is mathematically equivalent to a non-zero flux-response coefficient with respect to the diffusion coefficient for that species. The approach would be to greatly increase the size of one of the proteins, in order to obtain a significant decrease in the diffusion coefficient for that protein. The resulting change in the total pathway flux is an indication of the flux-response coefficient for that diffusion coefficient, and therefore of the concentration gradient. A major difficulty in this approach is, however, that the reaction rate constants are expected to change, and would have to be determined anew.

Acknowledgements
The research on which this paper reports has been carried out under the Biotechnology and Bioinformatics project of the Amsterdam Science and Technology Centre which is funded by the ICES-KIS program, and in collaboration with the Swammerdam Institute for Life Sciences of the University of Amsterdam. The authors wish to express their gratitude to Prof. dr. H. V. Westerhoff, dr. P. W. Postma, dr. C. Francke, and H. Brinkman for their continuing support and active participation in this research.

MODEL EXPERIMENTS

A $D_c = 60\,\mu\text{m}^2\ \text{min}^{-1}$ for all intracellular protein species and uniform in space.

B More crowding in cell-center.
$D_c(r) = 60/50\,\mu\text{m}^2\ \text{min}^{-1}$ for $0 <= r <= 0.5$ and $D_c(r) = 60\,\mu\text{m}^2\ \text{min}^{-1}$ for $0.5 <= r <= 1$ for all protein species.

C Diffusion of complexes much slower.
$D_c = 60\,\mu\text{m}^2\ \text{min}^{-1}$ for all uncomplexed proteins, and $D_c = 0.06\,\mu\text{m}^2\ \text{min}^{-1}$ for all complexes.

D Diffusion volume/mass dependent.
$D_c = \sqrt[3]{M(\text{HPr})/M(c)} \cdot 60\,\mu\text{m}^2\ \text{min}^{-1}$, where $M(c)$ is the mass of the protein species (cf. (5.2)).

E 'Large' label attached to HPr.
$M(\text{HPr}) \cdot 10$.

F 'Large' label attached to IIA.
$M(\text{IIA}) \cdot 10$.

	A	**B**	**C**	**D**	**E**	**F**	$D_c = 10^5$
IICB	0.74	0.75	0.53	0.79	0.75	1.04	0.47
IIA·P·IICB	1.66	1.65	1.80	1.63	1.65	1.47	1.82
IICB·P	0.04	0.04	0.04	0.03	0.04	0.03	0.04
IICB·P· Glc	0.90	0.90	0.96	0.88	0.89	0.79	1.00

Table 1: Distribution of membrane protein species[1].

	A	**B**	**C**	**D**	**E**	**F**	$D_c = 10^5$
J	54173	54091	58173	53236	53740	47924	60206
R^J_{EI}	0.11	0.11	0.07	0.12	0.12	0.15	0.05
R^J_{HPr}	-0.03	-0.03	0.00	-0.03	-0.02	-0.04	-0.02
R^J_{IIA}	0.33	0.33	0.19	0.35	0.32	0.48	0.17
R^J_{IICB}	0.72	0.72	0.86	0.69	0.71	0.53	0.91
$R^J_{D(\text{EI})}$	0.00	0.00	0.00	0.00	0.00	0.00	0.00
$R^J_{D(\text{HPr})}$	-0.02	-0.02	0.00	-0.03	-0.02	-0.06	0.00
$R^J_{D(\text{IIA})}$	0.09	0.08	0.02	0.10	0.08	0.17	0.00

Table 2: Steady-state properties of the model.
Flux J[1]and the flux-response coefficients of the four glucose PTS proteins and of the diffusion coefficients.

[1]Membrane species values are surface concentrations ($\mu\text{M}\,\mu\text{m}$). J denotes the (surface) flux per cell ($\mu\text{M}\,\mu\text{m}^3\ \text{min}^{-1} = 10^{-21}\text{mol min}^{-1}$). In [6] both the membrane species and the flux are expressed in μM, i.e. in volume concentrations. To compare our values with the ones in [6] the surface concentrations should be multiplied by $3/r$ and the flux divided by $4/3\,\pi r^3$, $r = 1\,\mu\text{m}$.

EI	0.27	EI·P·HPr	0.49	HPr·P·IIA	18.45
EI·P·Pyr	3.05	HPr	1.28	IIA	0.64
EI·P	1.19	HPr·P	29.78	IIA·P	15.43

Table 3: Distribution of intracellular protein species for $D_c = 10^5\,\mu\text{m}^2\ \text{min}^{-1}$.

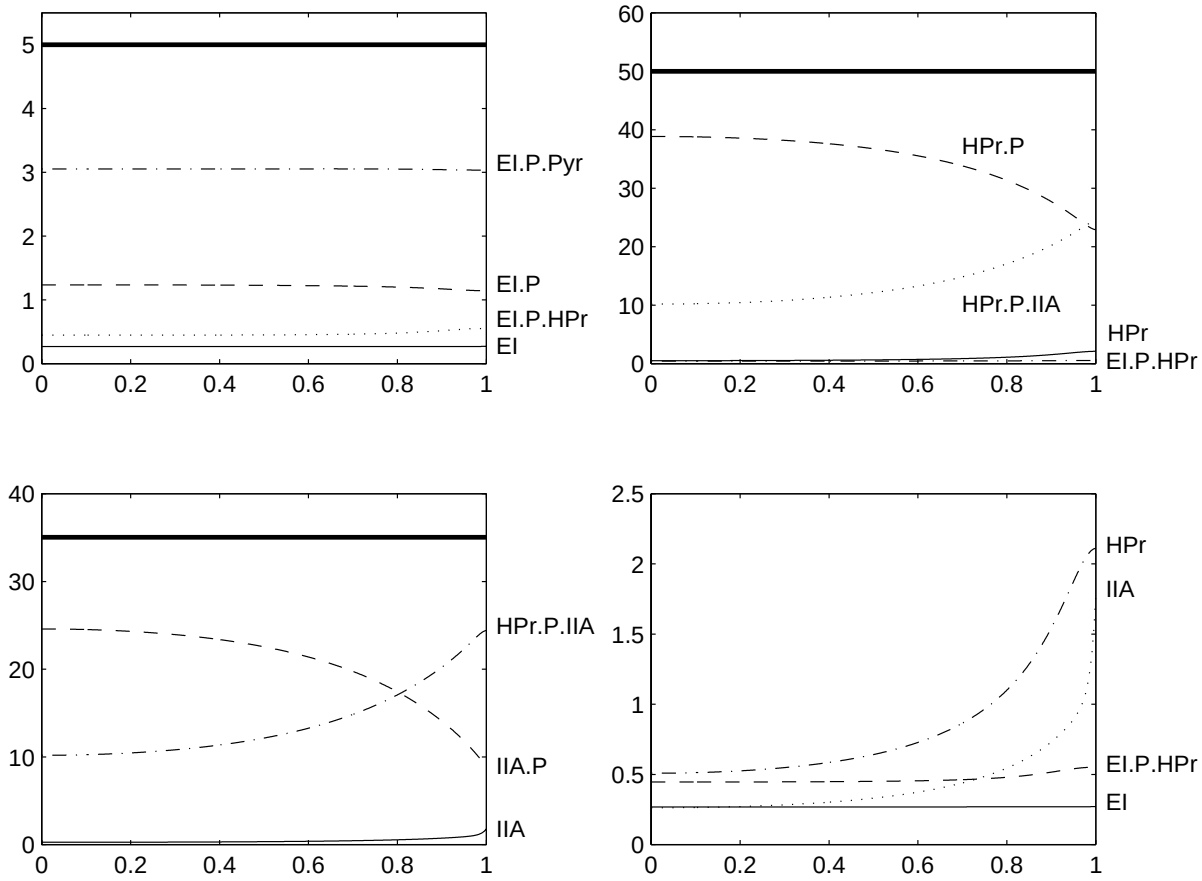

Figure 2: Experiment **A**: $D_c = 60\,\mu\text{m}^2\ \text{min}^{-1}$ for all protein species and uniform in space.

The fat line shows the total concentration for the specific protein, i.e., the sum of all other lines in the plot. Along the horizontal axis the distance from the center is given (μm), along the vertical axis the concentration values in μM.

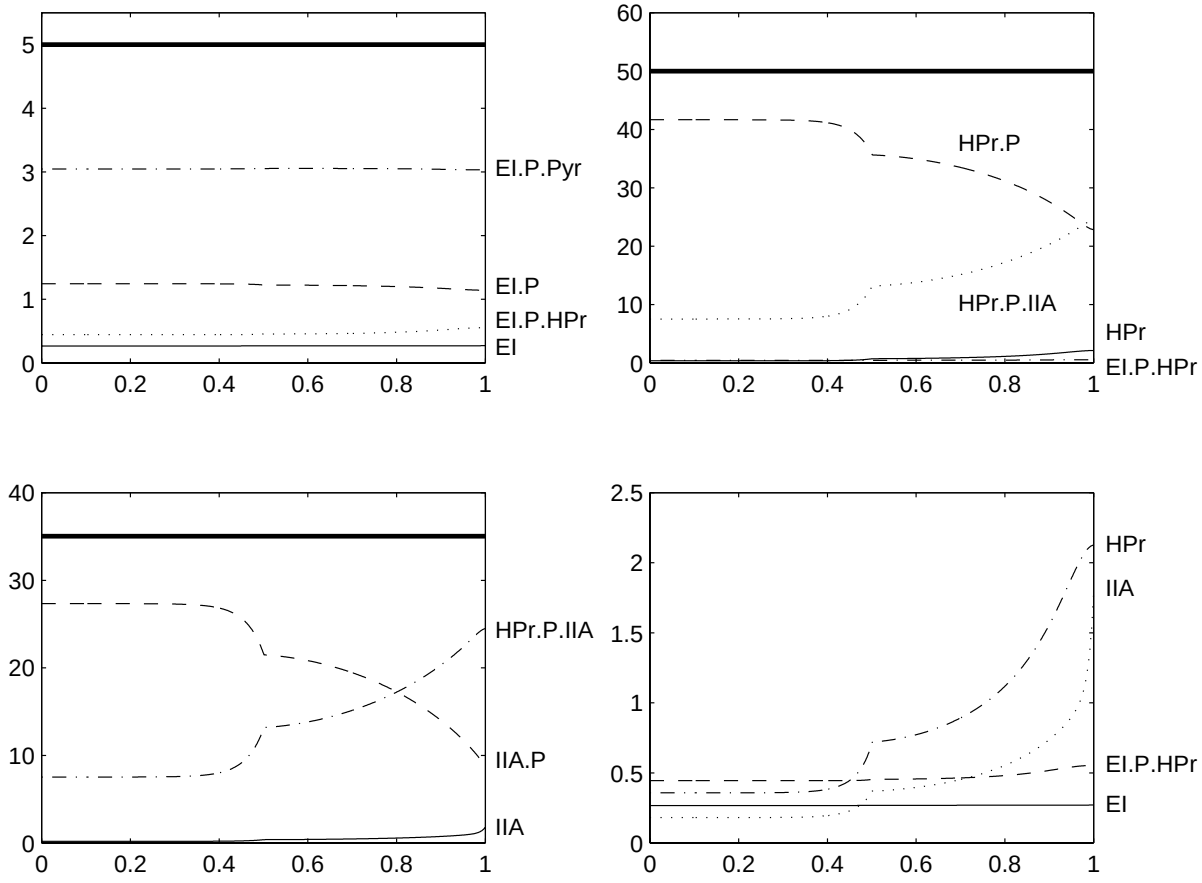

Figure 3: Experiment **B**: More crowding in cell-center.

The fat line shows the total concentration for the specific protein, i.e., the sum of all other lines in the plot. Along the horizontal axis the distance from the center is given (μm), along the vertical axis the concentration values in μM.

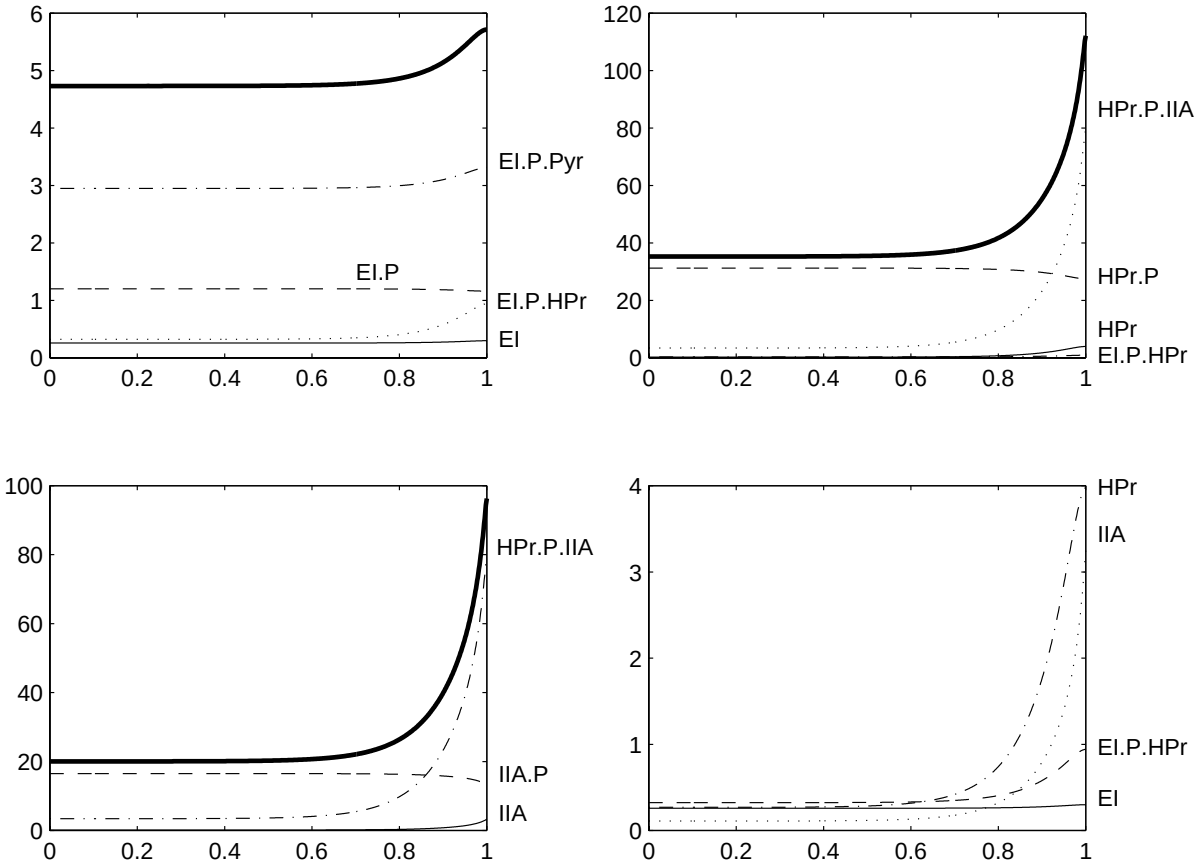

Figure 4: Experiment **C**: Diffusion of complexes much slower.

The fat line shows the total concentration for the specific protein, i.e., the sum of all other lines in the plot. Along the horizontal axis the distance from the center is given (μm), along the vertical axis the concentration values in μM.

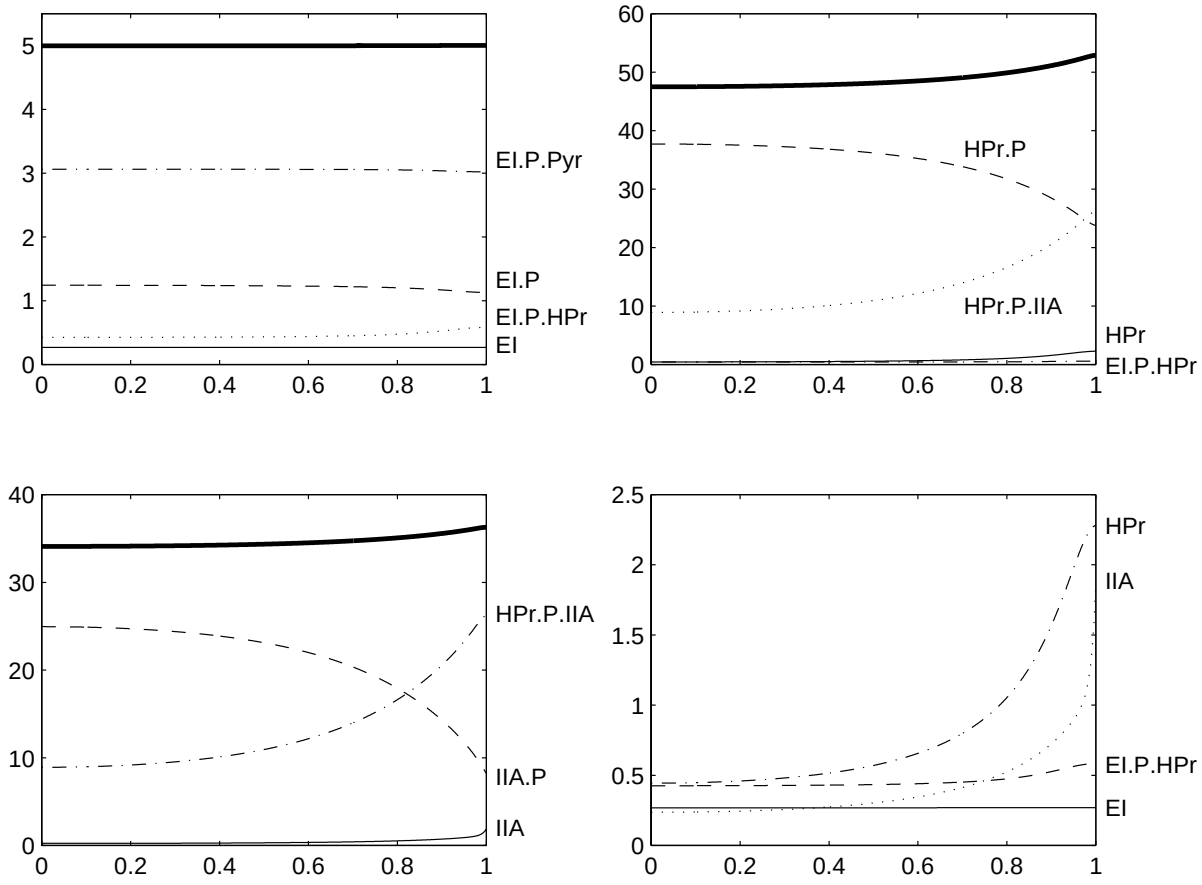

Figure 5: Experiment **D**: Diffusion volume/mass dependent.

The fat line shows the total concentration for the specific protein, i.e., the sum of all other lines in the plot. Along the horizontal axis the distance from the center is given (μm), along the vertical axis the concentration values in μM.

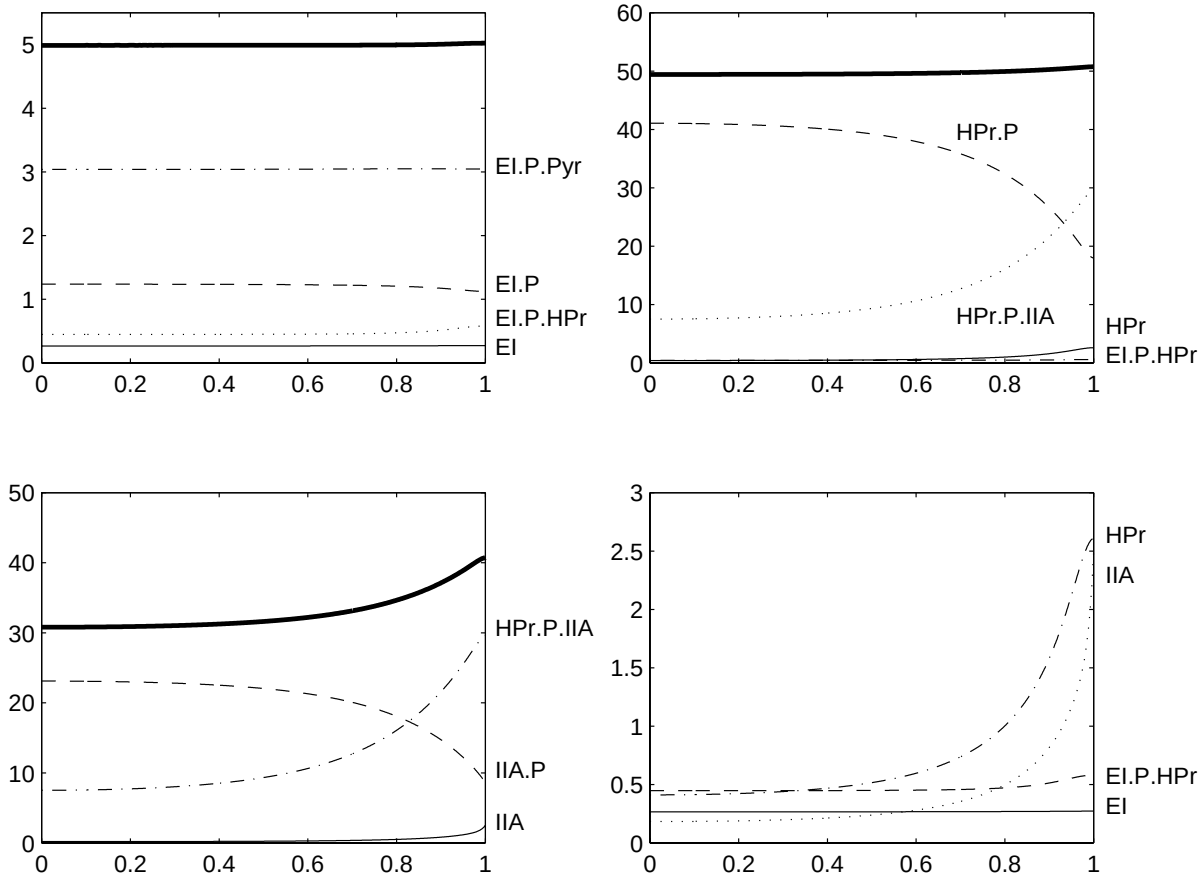

Figure 6: Experiment **E**: 'Large' label attached to HPr.

The fat line shows the total concentration for the specific protein, i.e., the sum of all other lines in the plot. Along the horizontal axis the distance from the center is given (μm), along the vertical axis the concentration values in μM.

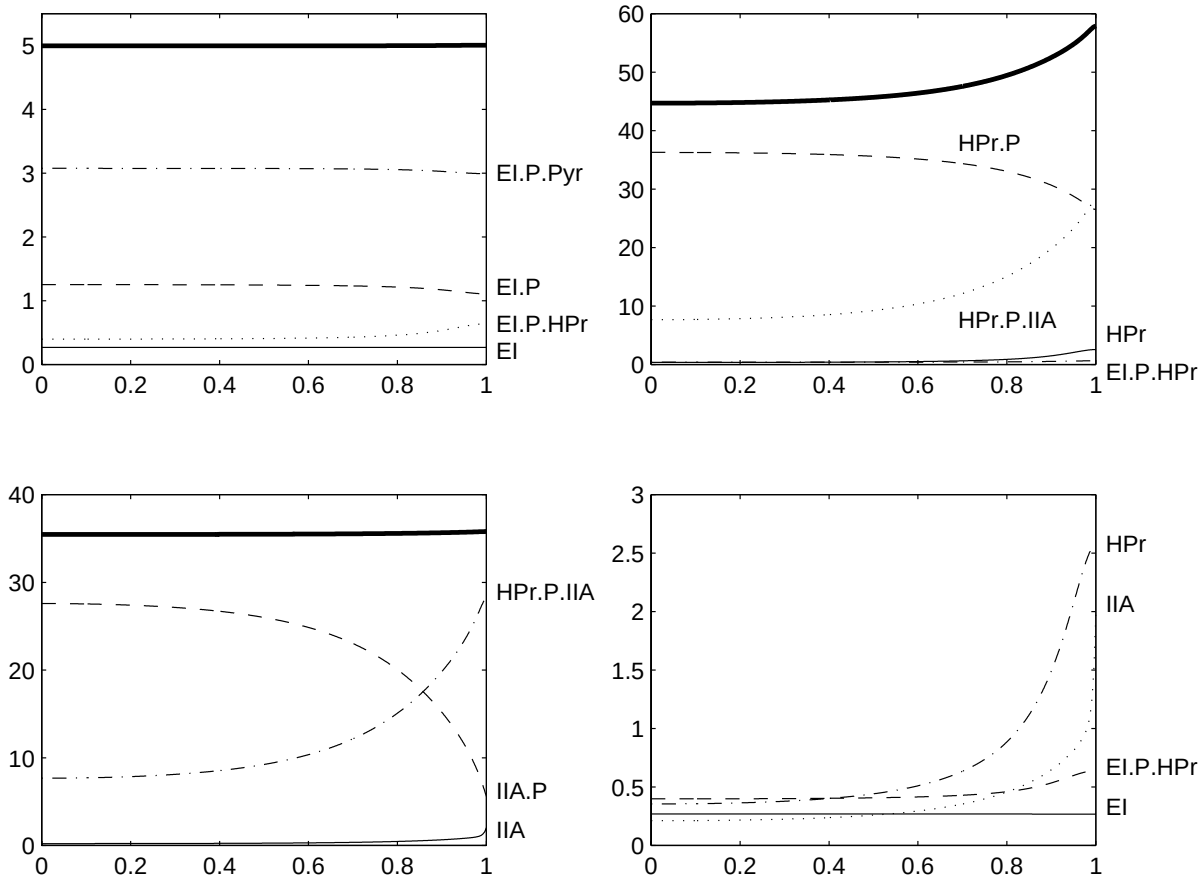

Figure 7: Experiment **F**: 'Large' label attached to IIA.

The fat line shows the total concentration for the specific protein, i.e., the sum of all other lines in the plot. Along the horizontal axis the distance from the center is given (μm), along the vertical axis the concentration values in μM.

Appendix

Parameter	Unit	Value	Parameter	Unit	Value
PTS protein concentrations			Boundary metabolite concentrations		
$[\mathrm{EI}]_{\mathrm{total}}$	μM	5	PEP	μM	2800
$[\mathrm{HPr}]_{\mathrm{total}}$	μM	50	Pyr	μM	900
$[\mathrm{IIA}]_{\mathrm{total}}$	μM	40	Glc	μM	500
$[\mathrm{IICB}]_{\mathrm{total}}$[2]	μM μm	3.33	Glc·P	μM	50
Rate constants (PTS step in parentheses)					
k_1 (PEP to EI)	$\mu\mathrm{M}^{-1}\,\mathrm{min}^{-1}$	1960	k_{-1} (PEP to EI)	min^{-1}	480000
k_2 (PEP to EI)	min^{-1}	108000	k_{-2} (PEP to EI)	$\mu\mathrm{M}^{-1}\,\mathrm{min}^{-1}$	294
k_3 (EI to HPr)	$\mu\mathrm{M}^{-1}\,\mathrm{min}^{-1}$	14000	k_{-3} (EI to HPr)	min^{-1}	14000
k_4 (EI to HPr)	min^{-1}	84000	k_{-4} (EI to HPr)	$\mu\mathrm{M}^{-1}\,\mathrm{min}^{-1}$	3360
k_5 (HPr to IIA)	$\mu\mathrm{M}^{-1}\,\mathrm{min}^{-1}$	21960	k_{-5} (HPr to IIA)	min^{-1}	21960
k_6 (HPr to IIA)	min^{-1}	4392	k_{-6} (HPr to IIA)	$\mu\mathrm{M}^{-1}\,\mathrm{min}^{-1}$	3384
k_7 (IIA to IICB)	$\mu\mathrm{M}^{-1}\,\mathrm{min}^{-1}$	880	k_{-7} (IIA to IICB)	min^{-1}	880
k_8 (IIA to IICB)	min^{-1}	2640	k_{-8} (IIA to IICB)	$\mu\mathrm{M}^{-1}\,\mathrm{min}^{-1}$	960
k_9 (IICB to Glc)	$\mu\mathrm{M}^{-1}\,\mathrm{min}^{-1}$	260	k_{-9} (IICB to Glc)	min^{-1}	389
k_{10} (IICB to Glc)	min^{-1}	4800	k_{-10} (IICB to Glc)	$\mu\mathrm{M}^{-1}\,\mathrm{min}^{-1}$	$5.4 \cdot 10^{-3}$

Table 4: Parameters of the kinetic model

[2] Membrane species values are surface concentrations (μM μm). In [6] $[\mathrm{IICB}]_{\mathrm{total}}$ is expressed in μM, i.e., in volume concentration. To compare our values with the ones in [6] the surface concentration should be multiplied by $3/r$, $r = 1\,\mu$m.

References

1. K.E. Brenan, S.L. Campbell, and L.R. Petzold. *Numerical Solution of Initial-Value Problems in Differential-Algebraic Equations*. North-Holland, New-York, 1989.
2. G.C. Brown and B.N. Kholodenko. Spatial gradients of cellular phospho-proteins. *FEBS Letters*, 457:452–454, 1999.
3. J.J. Dongarra and E. Grosse. Distribution of mathematical software via electronic mail. *Commun. ACM*, 30:403–407, 1987. (netlib@research.att.com).
4. M.B. Elowitz, M.G. Surette, P-E. Wolf, J.B. Stock, and S. Leibler. Protein mobility in the cytoplasm of *Escherichia coli*. *J. Bacteriol.*, 181(1):197–203, 1999.
5. J.M. Rohwer. *Interaction of functional units in metabolism. Control and regulation of the bacterial phosphoenolpyruvate-dependent phosphotransferase system.* PhD thesis, University of Amsterdam, the Netherlands, 1997.
6. J.M. Rohwer, N.D. Meadow, S. Roseman, H.V. Westerhoff, and P.W. Postma. Understanding glucose transport by the bacterial phosphoenolpyruvate:glycose phosphotransferase system on the basis of kinetic measurements *in vitro*. *To appear in J. Biol. Chem.*, 2000.